OCEANOGRAPHY

Emergence of the Central Atlantic Niño

Lei Zhang[1,2]*, Chunzai Wang[1,2]*, Weiqing Han[3], Michael J. McPhaden[4], Aixue Hu[5], Wen Xing[1]

The Atlantic Niño is characterized by sea surface warming in the equatorial Atlantic, which can trigger La Niña, the cold phase of El Niño–Southern Oscillation (ENSO). Although observations show that the Atlantic Niño has weakened by approximately 30% since the 1970s, its remote influence on ENSO remains strong. Here, we show that this apparent discrepancy is due to the existence of two types of Atlantic Niño with distinct patterns and climatic impacts, which we refer to as the central and eastern Atlantic Niño. Our results show that with equal strength, the central Atlantic Niño has a stronger influence on tropical climate than its eastern counterpart. Meanwhile, the eastern Atlantic Niño has weakened by approximately 50% in recent decades, allowing the central Atlantic Niño to emerge and dominate the remote impact on ENSO. Given the distinct climatic impacts of the two types, it is necessary to distinguish between them and investigate their behaviors and influences on climate in future studies.

INTRODUCTION

Climate conditions in the tropical Atlantic Ocean exhibit prominent year-to-year fluctuations, and its dominant mode is known as the Atlantic Niño or Niña, analogous to the Pacific El Niño and La Niña, the warm and cold phases of El Niño–Southern Oscillation (ENSO) (*1*, *2*). The Atlantic Niño is characterized by warm sea surface temperature (SST) anomalies (SSTAs) in the central and eastern equatorial Atlantic Ocean, weakened easterly trade winds, and higher-than-normal rainfall in the tropical Atlantic (*3*–*7*). The Atlantic Niña typically exhibits opposite anomalous signals (*8*).

The Atlantic Niño can prominently affect climate conditions in the surrounding continental regions, such as bringing more rainfall to Brazil (*9*), causing drought in the Sahel region (*10*), and affecting the African Easterly Jet (*11*). Its impacts also extend to remote regions. For instance, the Atlantic Niño can contribute to the development of La Niña in a few months by enhancing the Pacific Walker circulation (*12*–*16*), although the extent of this remote impact of the Atlantic Niño on ENSO remains a subject of ongoing debate (*17*, *18*). Similarly, ENSO's influence on the Atlantic Niño is also inconsistent (*19*–*21*). Moreover, the Atlantic Niño can weaken the Indian summer monsoon circulation, leading to reduced rainfall over India (*22*–*25*). In turn, the Indian Ocean climate anomalies may trigger the Atlantic Niño through the atmospheric teleconnection (*26*, *27*). Therefore, the Atlantic Niño is an important part of tropical interbasin interactions, and a better understanding of its climatic impact has important socioeconomic implications.

The Atlantic Niño has weakened substantially in the past few decades (Fig. 1C) (*28*, *29*). Variance of the ATL3, an index that has been used to measure the strength of the Atlantic Niño (*1*), has decreased by ~30% since 2000 [defined as period 2 (P2) in our study] compared to that during 1970–1999 [defined as period 1 (P1)]. Despite the much-weakened amplitude of the Atlantic Niño itself, its remote impact on ENSO has remained strong and steady since the 1970s (Fig. 1C) (*30*, *31*), and its influence on the Indian summer monsoon has actually strengthened in recent decades (*32*). Furthermore, a comparison between P1 and P2 reveals that the Atlantic Niño, as measured by the ATL3, not only weakens but also exhibits different main spatial patterns (Fig. 1, A and B). During P1, the warm SSTA extends from the western coasts of South Africa to the central equatorial Atlantic Ocean, whereas, in P2, the warming center is mainly located in the central basin with weak coastal warming.

The distinct Atlantic Niño pattern in recent decades seems to suggest that a different type of the Atlantic Niño, i.e., central Atlantic Niño, has emerged since ~2000, while the canonical Atlantic Niño or eastern Atlantic Niño seems to dominate before that. As the warm SSTA centers are located in different regions for the two types, they may have different climatic impacts. Here, we propose a method that defines and separates the central and eastern Atlantic Niño and provide observational evidence that the two types have distinct climatic impacts on both local and remote regions. In particular, the recently emerged central Atlantic Niño can have a stronger influence on ENSO. We explore the associated physical mechanisms by performing numerical experiments and analyzing results from multiple climate model simulations.

RESULTS

Central and eastern Atlantic Niño

To characterize the central and eastern Atlantic Niño separately and assess their respective climatic impacts, we first conducted empirical orthogonal function (EOF) analysis to extract dominant modes of tropical Atlantic climate variability (fig. S1). The first EOF mode (EOF1) exhibits prominent warm SSTA in both the central and eastern equatorial Atlantic Ocean, depicting the Atlantic Niño as a whole with its two types entangled together. The second mode (EOF2) exhibits a north-south dipole pattern that primarily corresponds to the Atlantic Meridional Mode (*33*), which is an important driver for the Atlantic Niño (*4*, *34*, *35*). The third mode (EOF3) portrays a zonal contrasting mode with opposite SSTA between the western-central equatorial Atlantic Ocean and the eastern basin.

[1]State Key Laboratory of Tropical Oceanography, South China Sea Institute of Oceanology, Chinese Academy of Sciences, Guangzhou, China. [2]Global Ocean and Climate Research Center, South China Sea Institute of Oceanology, Chinese Academy of Sciences, Guangzhou, China. [3]Department of Atmospheric and Oceanic Sciences, University of Colorado, Boulder, Colorado, USA. [4]National Oceanic and Atmospheric Administration/Pacific Marine Environmental Laboratory, Seattle, WA, USA. [5]National Center for Atmospheric Research, Boulder, CO, USA. *Corresponding author. Email: zhanglei@scsio.ac.cn (L.Z.); cwang@scsio.ac.cn (C.W.)

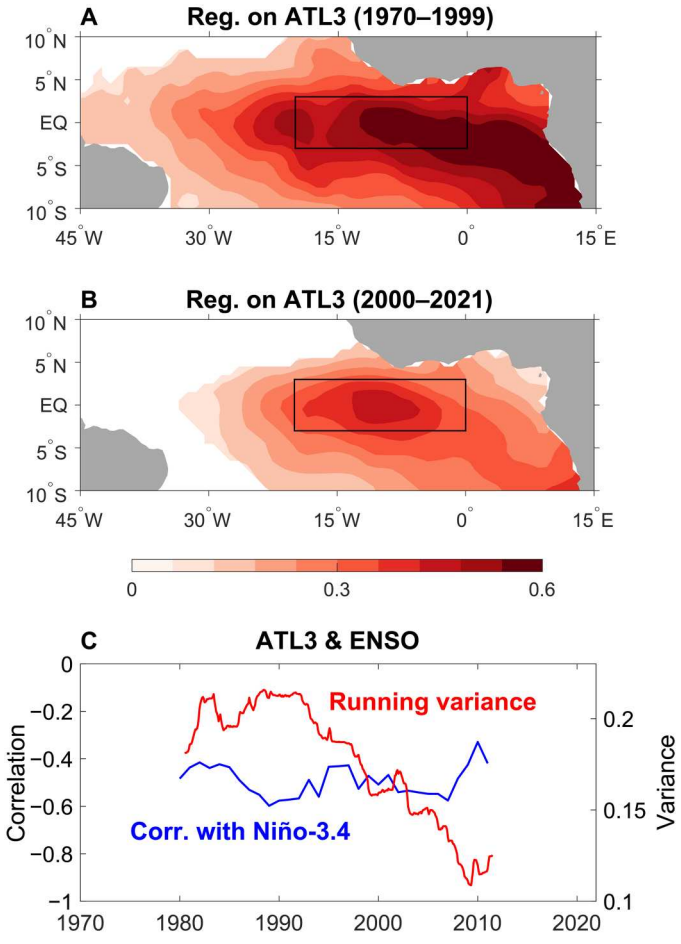

Fig. 1. Atlantic Niño before and after 2000. (**A**) Regression of June to August (JJA) mean SSTA on the normalized JJA ATL3 during 1970–1999. Unit is °C. The black box denotes the ATL3 region, 20°W-0°, 3°S-3°N. (**B**) Same as (A), but for 2000–2021. Results that are statistically significant at the 95% confidence level are shown. EQ, the equator. (**C**) Blue line denotes the 21-year running correlation between the JJA ATL3 and the December to February (DJF) Niño-3.4 index (left axis). Red line denotes the time evolution of the 21-year running variance of the ATL3 (right axis).

Note that the EOF1 captures both the central and eastern Atlantic Niño, while the EOF3 essentially depicts the dominant pattern of the zonal shift of the warm SSTA center. As the primary difference between the two types of the Atlantic Niño lies in the location of the maximum warming, we use different combinations of the two EOFs to represent the two types of the Atlantic Niño, which together account for ~60% of the total variance. Specifically, we define the spatial pattern of the eastern Atlantic Niño as $(\mathrm{EOF1}+\mathrm{EOF3})/\sqrt{2}$, which results in a pattern with strong warm SSTA located in the eastern equatorial Atlantic Ocean and along the western African coasts (Fig. 2A). In contrast, the spatial pattern of the central Atlantic Niño is obtained by calculating $(\mathrm{EOF1}-\mathrm{EOF3})/\sqrt{2}$, which shows the most prominent warming signals in the central equatorial Atlantic Ocean with weak coastal warming (Fig. 2B).

Accordingly, we also define central and eastern Atlantic Niño indices (CANI and EANI, respectively) by combining the two corresponding principal components (PCs) (see Materials and Methods) (Fig. 2C and fig. S1D). Both indices exhibit strong interannual variability, with evident differences between them during the analysis period. We further use the June to August (JJA) mean indices to define the years of the central and eastern Atlantic Niño. Here, we focus on boreal summer because it is the primary peak season of the Atlantic Niño as well as the main developing season of ENSO. We select 10 and 13 events for the central and eastern Atlantic Niño, respectively (see Materials and Methods). During the analysis period, there were only three mixed events when both types coexist (Fig. 2C), and these years have been excluded from further analysis. The results show that the occurrence of the eastern Atlantic Niño/Niña is less frequent during P2 compared to P1, while the frequency of the central Atlantic Niño/Niña started to increase since the mid-1990s compared with earlier periods (Fig. 2C). These inter-decadal changes in the relative strengths of the two types manifest as a shift in the Atlantic Niño pattern as has been noted in previous studies (*31*, *36*, *37*).

The composites of central and eastern Atlantic Niño events also reveal evident differences between the two types. During boreal summer, the eastern Atlantic Niño is characterized by prominent warming in the eastern basin, driven by westerly wind anomalies across the entire equatorial basin. In contrast, the central Atlantic Niño is accompanied by westerly wind anomalies in the western-central equatorial Atlantic Ocean with the strongest signals centered at 15°W (fig. S2 and Fig. 3). In addition, the central Atlantic Niño is associated with prominent warming in the central tropical South Atlantic Ocean. This SST warming is partly attributed to the northwesterly wind anomalies in the region, which weaken the southeasterly trades (fig. S2), reduce the surface wind speed, and thereby cause positive surface heat flux anomalies (fig. S3). In turn, the interhemispheric contrast of warm SSTA may enhance the northerly wind anomalies. Hence, the tropical South Atlantic warm SSTA may be an important precursor for the development of the central Atlantic Niño.

It has been shown that the formation of the Atlantic Niño is linked to a deepened thermocline and changes in ocean currents (*4*, *38*). Accordingly, the eastern type is associated with higher sea level east of 15°W as well as eastward current anomalies in the eastern basin, while the oceanic changes during the central type are primarily centered in the central basin with weaker anomalies across the equatorial Atlantic Ocean (fig. S4). Overall, the oceanic changes associated with the central Atlantic Niño are more pronounced than the eastern type, which are primarily driven by the more prominent wind forcing associated with the central type (fig. S2). Meanwhile, changes in surface heat fluxes tend to cause negative SSTA in the equatorial Atlantic Ocean and thus do not contribute to the development of either type (fig. S3), a result that is consistent with previous finding (*34*). Note that the distinct patterns between the central and eastern Atlantic Niño are not manifestations of inter-decadal changes in the Atlantic mean states, because the 8-year high-pass–filtered fields that isolate interannual variabilities show similar results (figs. S2 to S4).

Diverse climatic impacts

We next examine the impacts of the two types of the Atlantic Niño on local and remote climate. Note that the warm SSTA associated with the central Atlantic Niño is embedded in a higher background SST with strong east-west gradient compared to the eastern type

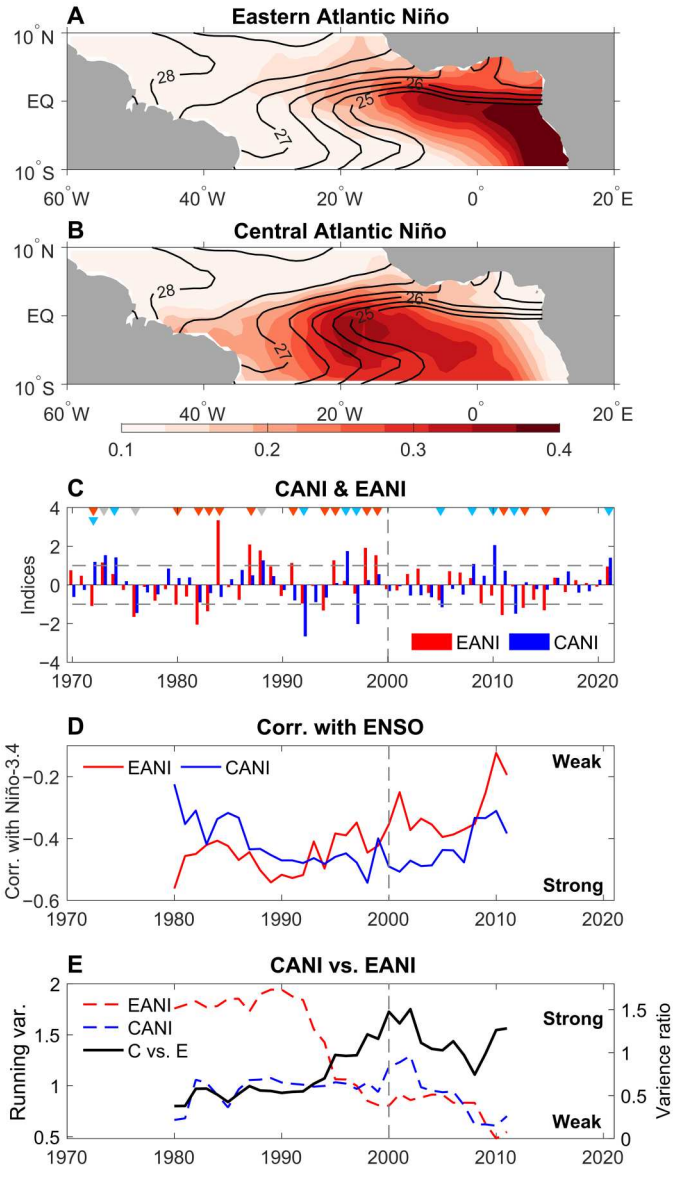

Fig. 2. Central and eastern Atlantic Niño. (**A**) Eastern Atlantic Niño SST anomaly pattern obtained as $(\mathrm{EOF1}+\mathrm{EOF3})/\sqrt{2}$ (shading, °C) (see Materials and Methods). Line contours represent the JJA SST climatology at a 0.5°C interval. Only SST higher than 25°C is shown to highlight the warm region. (**B**) Same as (A), except for the central Atlantic Niño defined as $(\mathrm{EOF1}-\mathrm{EOF3})/\sqrt{2}$. (**C**) Red and blue bars represent JJA mean eastern and central Atlantic Niño indices (EANI and CANI, respectively; left axis) (see Materials and Methods). Red and blue triangles at the top denote the selected eastern and central Atlantic Niño/Niña years, and gray triangles denote the three mixed events. Note that the year 1972 met the definitions for both the eastern Atlantic Niña and the central Atlantic Niño. Horizontal dashed lines denote the thresholds to define Atlantic Niño/Niña events. (**D**) Red line denotes 21-year running correlation coefficient between the JJA EANI and the DJF Niño-3.4 index. Blue for correlation coefficient between the CANI and the Niño-3.4. The vertical gray line denotes the year 2000. (**E**) Twenty-one-year running variance of the JJA EANI (red) and CANI (blue) (left axis). Black line denotes the variance ratio of the CANI and the EANI (right axis).

(Fig. 2, A and B), making it more effective at inducing atmospheric response due to the nonlinear dependence of convection and rainfall on SST in the tropics (*31*, *39*–*41*). Consistently, the central Atlantic Niño is associated with stronger tropical Atlantic rainfall anomalies than its eastern counterpart (fig. S5). As a result, the roles of the two Atlantic Niño types in driving the atmospheric teleconnection and thereby affecting other tropical ocean basins may differ. The central Atlantic Niño has a strong influence on ENSO throughout the analysis period, whereas the effect of the eastern type has substantially weakened (Fig. 2D). These findings are in agreement with earlier studies that reported a more prominent impact of the western equatorial Atlantic Ocean than the eastern basin on ENSO (*31*, *36*).

The divergent changes in the remote influences of the two Atlantic Niño types over the past few decades can be attributed to changes in the ratio of their strengths. In the 1970s and 1980s, the variance of the EANI was almost twice as strong as the CANI (Fig. 2E), allowing the warm SSTA associated with the eastern Atlantic Niño to induce prominent atmospheric changes, despite being located in the Atlantic cold tongue region where the background SST is low (Fig. 2A). Consequently, both types could induce notable local rainfall variations and affect remote regions via atmospheric teleconnection during P1 (fig. S5, E and G). However, since the early 1990s, the variance of the EANI has been rapidly weakening and reached a weak value near 2000, while the variance of the CANI has remained relatively stable, leading to similar variances for the two indices since the late 1990s (Fig. 2E). As a result, the eastern type has weak impact on local and remote climate (fig. S5F), and the role of the Atlantic Niño in interbasin interactions is mainly driven by the central Atlantic Niño (fig. S5H).

To better illustrate the diverse impacts of the central and eastern Atlantic Niño on ENSO, we examine the Pacific SST and wind anomalies induced by them during P1 and P2 (Fig. 3). The results show that both types induce strong easterly wind anomalies and cold SSTA in the tropical Pacific Ocean during P1, contributing to the development of La Niña. This interbasin connection is particularly evident in the upper troposphere, where the easterly wind anomalies induced by the Atlantic Niño extend from the tropical Atlantic Ocean to South America and the eastern tropical Pacific Ocean, thus affecting the Pacific Walker circulation (fig. S5, A and C). However, during P2, the impact of the eastern type on ENSO has diminished because of its much weaker amplitude, whereas the role of the central Atlantic Niño remains strong (Fig. 3 and fig. S5), consistent with findings above. Also note that the Atlantic Niño weakens after its peak in summer, while the development of La Niña continues (Fig. 3), owing to local atmosphere-ocean interactions in the tropical Pacific Ocean.

Recent studies have suggested that the development of ENSO, because of its autocorrelation or its quasi-biennial cycle, could be misinterpreted as being forced by remote influences from other basins (*17*, *42*). To investigate this hypothesis, we further examine preceding spring and winter seasons before the Atlantic Niño peak and find that there are negligible or statistically insignificant signals in the tropical Pacific Ocean during those periods (fig. S6). This result suggests that the subsequent development of ENSO after the Atlantic Niño peak is triggered by the Atlantic Niño.

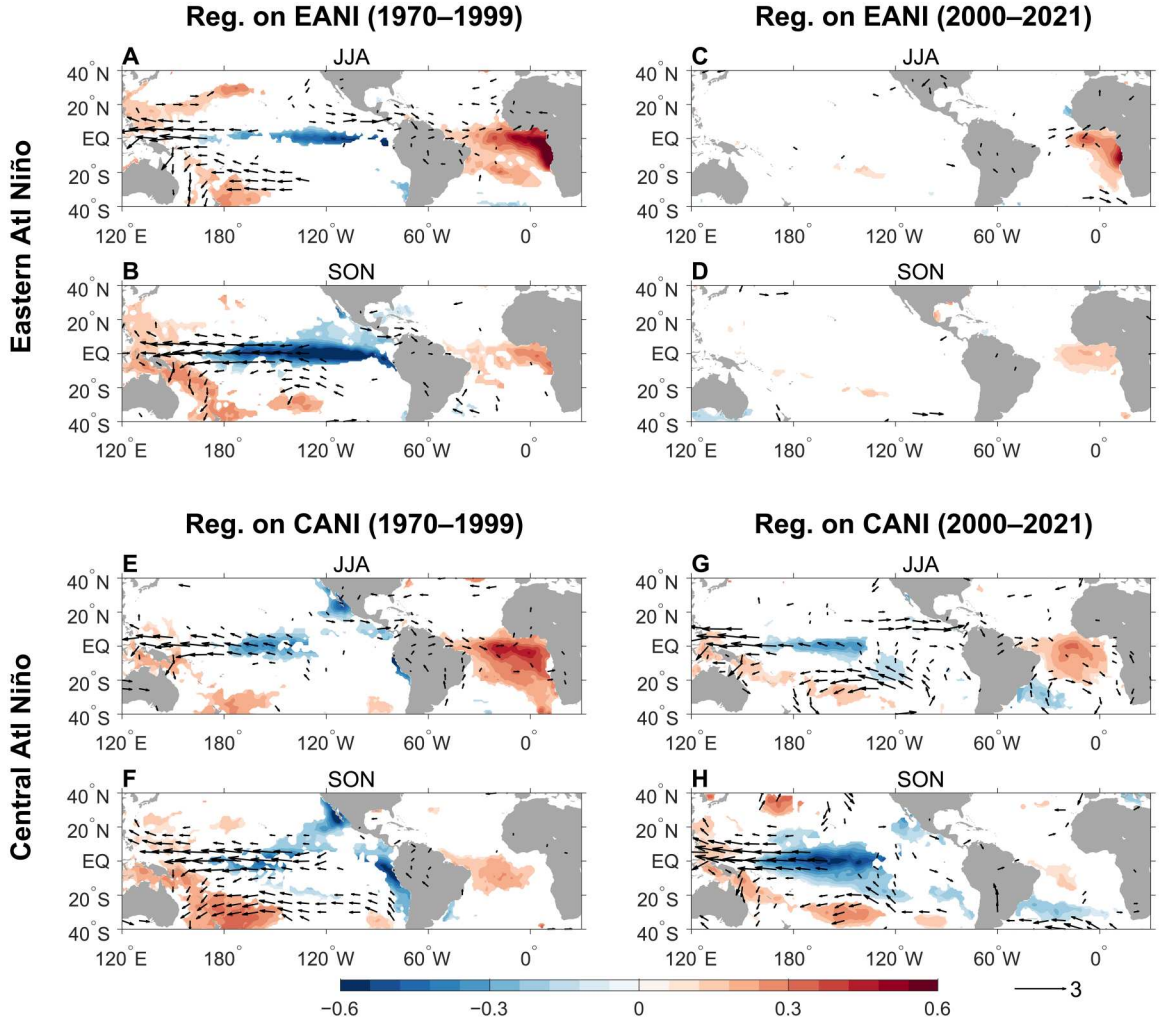

Fig. 3. Pacific climate anomalies associated with the Atlantic Niño. (**A**) Regression of JJA mean SST (shading, °C) and 850-hPa wind (vector, m s^{-1}) anomalies on the normalized JJA EANI during 1970–1999. Results that are statistically significant at the 95% confidence level are shown. (**B**) Same as (A), but for regression of the September to November (SON) mean anomalies on the normalized JJA EANI. (**C** and **D**) Same as (A) and (B), but for results during 2000–2021. (**E** to **H**) Same as (A) to (D), but for regression on the normalized JJA CANI.

Numerical model experiments

To further confirm the different impacts of the central and eastern Atlantic Niño on tropical climate, we conduct atmospheric general circulation model (AGCM) experiments, where the tropical Atlantic SSTAs associated with each of the two types of the Atlantic Niño are used as forcings (see Materials and Methods; Fig. 4, A and D). Our focus is on the triggering effect of the Atlantic Niño on ENSO during its peak in boreal summer because further development of the Pacific anomalies in the following seasons is a result of local atmosphere-ocean interactions that cannot be captured by the AGCM. Our model experiments show that, in the western tropical Atlantic Ocean, the central Atlantic Niño induces stronger positive rainfall anomalies than its eastern counterpart, while the latter is associated with more prominent rainfall anomalies in the eastern basin and the region to the south of the Sahel (Fig. 4, B and E). As a result, the central Atlantic Niño leads to prominent westerly wind anomalies in the tropical Atlantic Ocean and the eastern tropical Pacific Ocean, as well as easterly wind anomalies over the western-central tropical Pacific Ocean, especially around 180°, that favor the development of La Niña (Fig. 4F) (*43*). On the other hand, the eastern Atlantic Niño has rather weak influence on the Pacific wind anomalies (Fig. 4C). These results suggest stronger climatic impacts of the central Atlantic Niño, which are consistent with observations.

We conduct further analysis using historical simulations from multiple state-of-the-art climate models that participate in Coupled Model Intercomparison Project Phase 6 (CMIP6) (see Materials and Methods) (*44*). In contrast to the AGCM experiments, the atmosphere and ocean are fully coupled in CMIP6 climate models, which allows for more realistic representations of the Atlantic Niño impact on ENSO, including the further development of ENSO during the Atlantic Niño decaying phase. The results show that the CMIP6 models can capture the two types of the Atlantic Niño to some extent, although they tend to underestimate the warm SSTA along the western African coasts during the eastern Atlantic Niño, which could be attributed to model biases in simulating

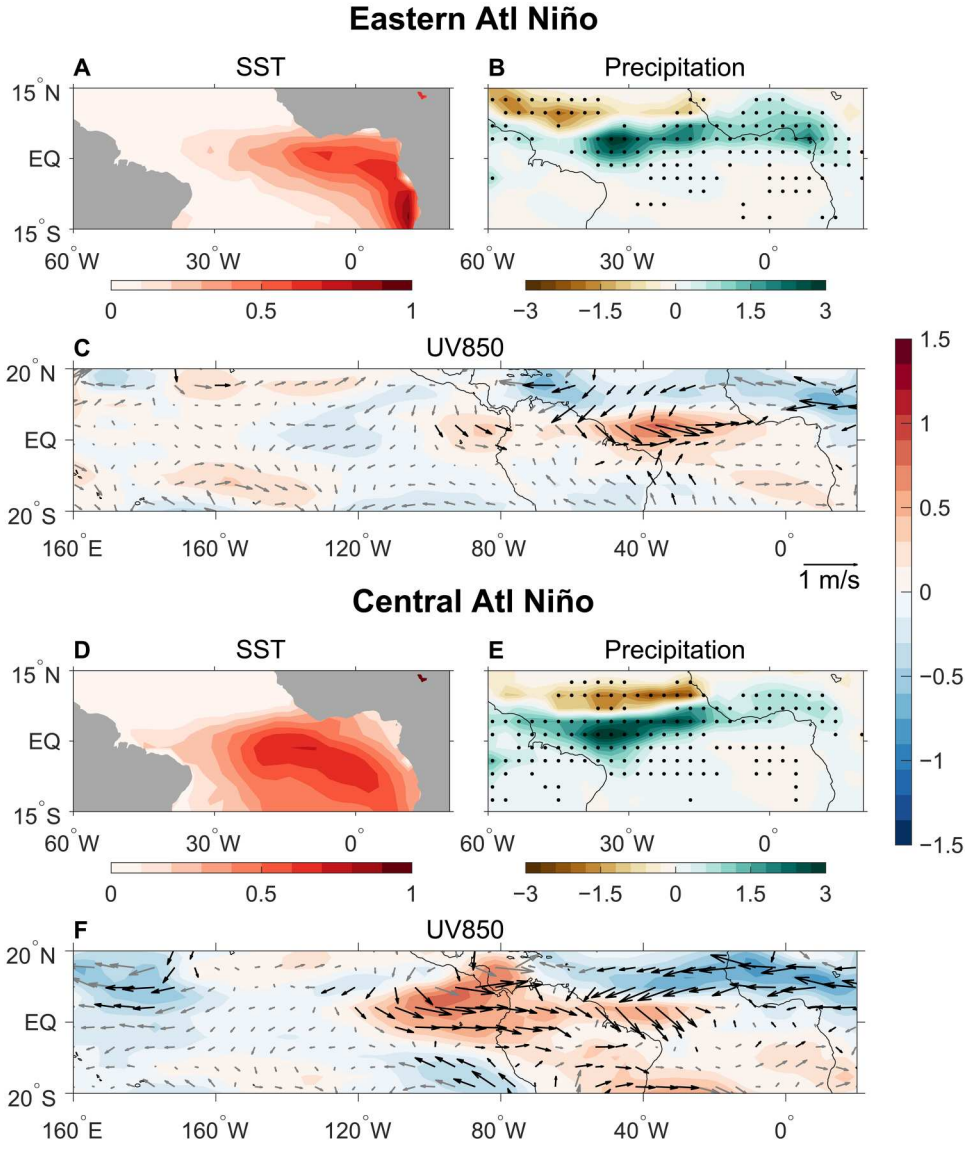

Fig. 4. Atmospheric model experiments. Differences of JJA mean (**A**) SST (°C), (**B**) precipitation (shading, mm day^{-1}), and (**C**) 850-hPa wind (vector, m s^{-1}) and zonal wind (shading, m s^{-1}) between the eastern Atlantic Niño experiment and the control run (see Materials and Methods). Stippling and black vectors in (B) and (C) represent results that are statistically significant at the 95% confidence level. (**D** to **F**) Same as (A) to (C), but for the central Atlantic Niño experiment.

the coastal processes that give rise to the coastal warming (fig. S7, A and E). In addition, this model bias could be also linked to the coastal warming bias in climate models (*45*), which may result in an underestimation of the meridional temperature gradient in the eastern tropical Atlantic Ocean as well as the anomalous meridional heat transport. However, despite these limitations, the models also show that the central Atlantic Niño induces prominent cold SSTA in the tropical Pacific Ocean, whereas the remote influence of the eastern type is weak (fig. S7), which is consistent with observations. In addition, we analyze 1300-year-long simulations from one single model, in which the external forcing (both natural and anthropogenic) is excluded (see Materials and Methods). The model produces results that are similar to observations (fig. S8), including the distinct patterns of the two types of the Atlantic Niño, as well as their diverse impacts on ENSO.

Weakening of the Atlantic Niño

The contrasting climatic impacts of the two Atlantic Niño types in observations are partly associated with the weakened eastern Atlantic Niño that leads to the muted ENSO response to the eastern type in recent decades (Fig. 2, D and E). Previous studies have attributed the weakening of the Atlantic Niño to the negative-to-positive phase transition of the Atlantic Multidecadal Oscillation (*36*, *37*, *46*, *47*) and hemispheric cooling contrast due to anthropogenic aerosols (*28*). It has also been shown that the Atlantic Niño may continue to weaken in the future under the influence of increases in the anthropogenic emission of greenhouse gases (*48*, *49*).

The suppressed Atlantic Niño variability is caused by the deepening of the thermocline, which weakens the sensitivity of SST to thermocline anomalies (*48*–*50*). The observed trend of upper-ocean temperature shows the strongest warming in the surface

layer of the eastern equatorial Atlantic Ocean (Fig. 5A), suggesting a deepening of the thermocline. Consequently, the variations in the thermocline have a weaker influence on SST during the Atlantic Niño developing phase in P2 compared to P1 (Fig. 5B), which weakens the strength of the Atlantic Niño. It should be noted that the thermocline is shallower in the eastern basin where the deepening is more prominent (Fig. 5A). Therefore, the weakened thermocline-SST feedback during P2 may more effectively suppress the eastern Atlantic Niño compared to the central Atlantic Niño. During P1, on the other hand, the thermocline in the eastern tropical Atlantic Ocean is relatively shallow, which creates favorable conditions for the formation of the eastern Atlantic Niño. As a result, the eastern type of Atlantic Niño occurs more frequently than the central type during P1. This is consistent with the fact that the weakening of the tropical Atlantic SST variance in P2 compared with P1 is more pronounced in the eastern basin than in the central basin (fig. S9, A to C).

On the other hand, the tropical Atlantic Ocean has experienced prominent warming since 1970 (Fig. 5A). This rise in SST may promote atmosphere-ocean coupling processes in recent decades, strengthening the role of the central Atlantic SSTA in driving local wind changes during its mature phase (Fig. 5C). This is consistent with the slightly weakened central Atlantic Niño in P2 and its similar influence on ENSO for both P1 and P2 although the SSTA is weaker in P2 (Fig. 3, E to H). Hence, changes in the tropical Atlantic mean states are crucial in modulating the relative importance of the two Atlantic Niño types and their climatic impacts.

DISCUSSION

The central and eastern Atlantic Niño are both characterized by equatorial Atlantic warming on interannual timescale but with different locations of the warmest SSTAs. The two types can be distinguished from each other by combining the EOF1 and EOF3 modes of equatorial Atlantic SSTA to describe the zonal shift of the respective warming centers. Because both types show prominent SSTA in the ATL3 region and are phase-locked to boreal summer (fig. S10), using only the traditional ATL3 index cannot properly separate signals associated with them.

Previous studies have identified various types of the Atlantic Niño. For instance, it has been found that the "noncanonical" Atlantic Niño (*34*) is caused by warm SSTA north of the equator that is

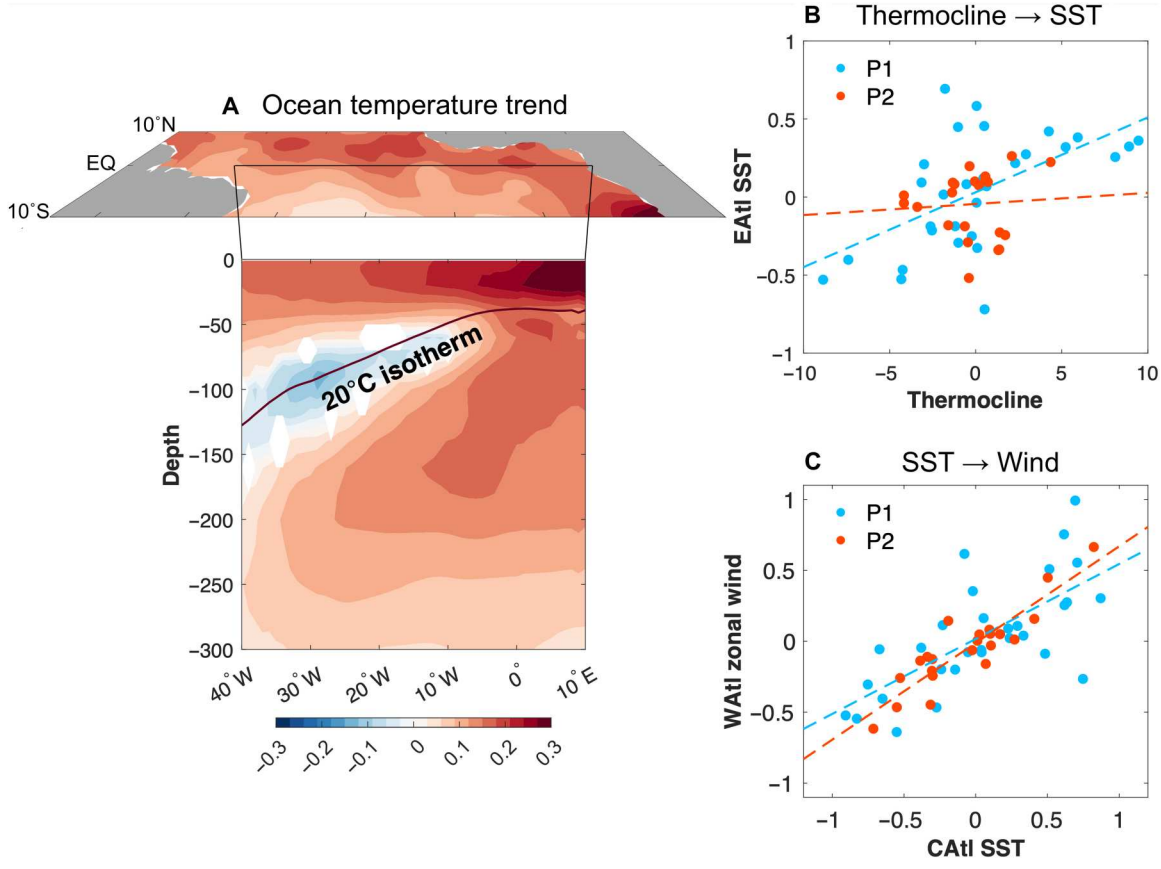

Fig. 5. Weakening of the Atlantic Niño. (**A**) Trends of SST from HadISST (top) and upper-ocean temperature averaged between 3°S and 3°N from IAP (bottom) during 1970–2021. Unit is °C decade^{-1}. Black curve in the lower panel indicates the depth of thermocline during boreal summer, defined as the 20°C isotherm. Results that are statistically significant at the 95% confidence level are shown. (**B**) Scatter plot between March to May (MAM) mean thermocline depth anomalies and SST anomalies averaged over the eastern equatorial Atlantic Ocean (3°S-3°N, 10°W-10°E). MAM is the developing season of the Atlantic Niño. (**C**) Scatter plot between JJA mean SST anomalies in the central equatorial Atlantic Ocean (3°S-3°N, 20°W-0°) and surface zonal wind anomalies averaged over the western equatorial Atlantic Ocean (3°S-3°N, 40°W-20°W). Blue and red dots represent results during P1 (1970–1999) and P2 (2000–2021), respectively. Dashed lines denote the linear regression between the two variables.

advected toward the equator, which is different from the canonical Atlantic Niño driven by equatorial westerly wind anomalies. The noncanonical type exhibits a somewhat similar pattern to the central Atlantic Niño, but the latter is mainly associated with warming in the South Atlantic Ocean (fig. S2). In addition, the "late-onset" Atlantic Niño (*7*) also has a maximum warming in the central basin, but it seems that there is no notable difference in the onset timing between the central and eastern Atlantic Niño (fig. S2). Nevertheless, these previous findings may provide insight into understanding the distinct formation mechanisms of the two Atlantic Niño types. It should also be noted that both the central and eastern Atlantic Niño show a secondary peak in boreal winter (fig. S10), which suggests that they could be partly linked to the Atlantic Niño II that peaks in November and December (*51*).

It has also been shown that the Atlantic Niño is preceded by the Benguela Niño in some years (*52*, *53*), which is characterized by coastal warming along the western coasts of Africa (fig. S11). The peak of the eastern Atlantic Niño also shows prominent warming in the Benguela Niño region, whereas the Benguela Niño seems to lead the central Atlantic Niño by 2 to 3 months (figs. S2 and S11). The relationships between the two Atlantic Niño types and the Benguela Niño will be investigated in a future study. Note that, although the EOF3 has a large loading along the western African coasts at 10° S (fig. S1C), its correlation with the Benguela Niño is weak (fig. S11E). This is because the Benguela Niño primarily exhibits same-sign changes in the equatorial Atlantic SSTA (fig. S11), while EOF3 is associated with opposite SSTA between the western and eastern basin.

The emergence of the central Atlantic Niño in recent decades can be attributed to the weakening of its eastern counterpart by ~50% since the 1970s, resulting in comparable variance between the EANI and the CANI after the mid-1990s. Despite the overall weaker variance of the CANI over the analysis period, the central Atlantic Niño can still affect local and remote climate during both P1 and P2 because its warmest SSTA is embedded in a higher background SST than the eastern type. These findings explain the steady and strong relationship between the Atlantic Niño and ENSO since the 1970s, despite the substantially weakened ATL3 variance (Fig. 1C). In other words, the remote influence of the Atlantic Niño on ENSO after 2000 mainly originates from the central Atlantic Niño, while changes in the eastern Atlantic Niño are primarily responsible for the overall weakening of the Atlantic Niño.

Previous studies have also demonstrated an inter-decadal shift in the Atlantic Niño pattern in the 1970s, which may result in different impacts on ENSO due to variations in the location of the maximum SSTA variance center (*31*, *36*). Such inter-decadal change could be a manifestation of variations in the relative strengths of the two Atlantic Niño types. However, note that these two phenomena are linked to each other but not entirely equivalent, because the two Atlantic Niño types coexist with distinct behaviors throughout the study period and may occur alternately during certain periods such as the 1990s and the 2010s (Fig. 2C). In other words, the two types may represent two different flavors of the Atlantic Niño rather than a manifestation of the inter-decadal changes in the Atlantic Niño characteristics.

The weakening of the Atlantic Niño is attributed to the deepening of the thermocline that weakens the thermocline-SST feedback, which may more effectively suppress the eastern type. As a result, the variance ratio between the central and the eastern Atlantic Niño indices has increased prominently in the past few decades (Fig. 2E). Given the prominent climatic impacts of the central Atlantic Niño, the overall reduced variance of the Atlantic Niño at present and likely in the future does not necessarily translate into weaker influence on the tropical climate. Therefore, it is necessary for future studies to distinguish between the two types and investigate their distinct behaviors and climatic influences.

MATERIALS AND METHODS

Observational data

To characterize the Atlantic Niño and examine associated atmospheric and oceanic changes, we analyzed the monthly SST data from the Hadley Centre Sea Ice and SST (HadISST) (*54*); 850-hPa wind, precipitation, and surface heat flux data from European Centre for Medium-Range Weather Forecasts (ECMWF) Reanalysis 5 (ERA5) (*55*); and sea level and ocean current data from ECMWF Ocean Reanalysis System 5 (ORAS5) (*56*). Gridded ocean temperature analysis from Institute of Atmospheric Physics (IAP) (*57*) was used to analyze the upper ocean temperature trend. The analysis period was 1970–2021. Because of the sparse observations during the earlier period, which may have led to relatively large uncertainties (*58*), we did not use the observational data before 1970. All anomaly fields were linearly detrended to remove the influence of the anthropogenic greenhouse gas warming.

To document time evolution of ENSO and the Atlantic Niño, we calculated the Niño-3.4 index and the ATL3 index defined as SSTA averaged over 5°S-5°N, 170°W-120°W and 3°S-3°N, 20°W-0°, respectively. In addition, we performed linear regressions of various variables on the climate indices to obtain climate anomalies associated with the tropical climate modes. We evaluated the statistical significance of the obtained results using the two-sided Student's *t* test.

To identify the main patterns of tropical Atlantic climate variability, we conducted an EOF analysis on the monthly SSTA over 60°W-20°E, 10°S-10°N. The resulting PCs were normalized by their respective SDs, which are used to scale the corresponding EOFs. The EOF1 mode describes the Atlantic Niño as a whole, with the warm SSTA in both the central and eastern equatorial Atlantic Ocean. The EOF3 is a zonal contrasting mode associated with an east-west shift of the warming center. Therefore, we defined the eastern Atlantic Niño as $(\mathrm{EOF1}+\mathrm{EOF3})/\sqrt{2}$ and the central Atlantic Niño as $(\mathrm{EOF1}-\mathrm{EOF3})/\sqrt{2}$. A similar approach has been used to differentiate between the central and eastern Pacific ENSO in previous studies (*59*–*61*). Accordingly, we defined the EANI and CANI as $(\mathrm{PC1}+\mathrm{PC3})/\sqrt{2}$ and $(\mathrm{PC1}-\mathrm{PC3})/\sqrt{2}$, respectively. These definitions ensure that the sum of the central and eastern Atlantic Niño equals the sum of the two EOF modes, PC1 × EOF1 + PC3 × EOF3.

Atmospheric model experiments

To investigate the potential differences in the impacts of the two types of Atlantic Niño on local and remote climate, we conducted three AGCM experiments using ECHAM4.6 from Max Planck Institute in Hamburg (*62*). The model has a resolution of approximately 2.8° with 19 vertical levels. Each experiment was run for 42 years, with the first 4 years discarded to allow the model to

reach equilibrium. This resulted in a total of 38 members for our analysis.

In the control run, we forced the model with monthly SST climatology obtained from HadISST during 1970–2021. In the two sensitivity experiments, we added composited monthly SSTA during a 12-month period for the central and eastern Atlantic Niño in the tropical Atlantic Ocean between 22.5°S and 7.5°N, respectively. A sponge layer was added at the northern and southern boundaries. In this study, we defined the central Atlantic Niño (Niña) years as when the JJA mean CANI exceeded (fell below) 1 SD of the CANI over the analysis period. We chose JJA as it is the peak season of the Atlantic Niño as well as the developing season of ENSO (see fig. S10). A similar criterion was applied to identify eastern Atlantic Niño and Niña events. We excluded years when both types of Atlantic Niño/Niña occurred. The SSTA forcing fields for the two sensitivity experiments are then constructed as the differences between Niño and Niña years divided by two.

Climate model simulations

Given the relatively short observational record, we further analyzed climate model simulations to examine and compare the two types of the Atlantic Niño with a larger sample size. We first examine the monthly SST data from 20 CMIP6 models (table S1), including the historical simulations during 1970–2014 and future projections during 2015–2020 under Shared Socioeconomic Pathway 5–based Representative Concentration Pathway 8.5 forcing scenario (*63*). All model outputs are interpolated onto a common 1° × 1° grid. Some of the CMIP6 models have multiple ensemble members, results from which are averaged before calculating multimodel mean signals. In addition, we also analyze 1300-year-long preindustrial control simulations from the National Center for Atmospheric Research Community Climate System Model version 4 (CCSM4) (*64*), in which the effect of the natural and the anthropogenic external forcing was excluded.

Supplementary Materials

This PDF file includes:

Figs. S1 to S11
Table S1

REFERENCES AND NOTES

1. S. E. Zebiak, Air–sea interaction in the equatorial atlantic region. *J. Climate* **6**, 1567–1586 (1993).
2. M. J. McPhaden, S. E. Zebiak, M. H. Glantz, ENSO as an integrating concept in earth science. *Science* **314**, 1740–1745 (2006).
3. I. Richter, H. Tokinaga, "The Atlantic zonal mode: Dynamics, thermodynamics, and teleconnections" in *Tropical and Extratropical Air-Sea Interactions*, S. K. Behera, Ed. (Elsevier, 2021), pp. 171–206; https://linkinghub.elsevier.com/retrieve/pii/B9780128181560000083.
4. J. F. Lübbecke, Tropical Atlantic warm events. *Nat. Geosci.* **6**, 22–23 (2013).
5. N. S. Keenlyside, M. Latif, Understanding equatorial atlantic interannual variability. *J. Climate* **20**, 131–142 (2007).
6. J. A. Carton, B. Huang, Warm events in the tropical atlantic. *J. Phys. Oceanogr.* **24**, 888–903 (1994).
7. I. Vallès-Casanova, S. Lee, G. R. Foltz, J. L. Pelegrí, On the spatiotemporal diversity of atlantic niño and associated rainfall variability over West Africa and South America. *Geophys. Res. Lett.* **47**, e2020GL087108 (2020).
8. J. F. Lübbecke, M. J. McPhaden, Symmetry of the Atlantic Niño mode. *Geophys. Res. Lett.* **44**, 965–973 (2017).
9. C. K. Folland, A. W. Colman, D. P. Rowell, M. K. Davey, Predictability of Northeast Brazil rainfall and real-time forecast skill, 1987–98. *J. Climate* **14**, 1937–1958 (2001).
10. A. Giannini, R. Saravanan, P. Chang, Oceanic forcing of sahel rainfall on interannual to interdecadal time scales. *Science* **302**, 1027–1030 (2003).
11. T. Losada, B. Rodríguez-Fonseca, S. Janicot, S. Gervois, F. Chauvin, P. Ruti, A multi-model approach to the Atlantic Equatorial mode: Impact on the West African monsoon. *Climate Dynam.* **35**, 29–43 (2010).
12. B. Rodríguez-Fonseca, I. Polo, J. García-Serrano, T. Losada, E. Mohino, C. R. Mechoso, F. Kucharski, Are Atlantic Niños enhancing Pacific ENSO events in recent decades? *Geophys. Res. Lett.* **36**, L20705 (2009).
13. I. Polo, M. Martin-Rey, B. Rodriguez-Fonseca, F. Kucharski, C. R. Mechoso, Processes in the Pacific La Niña onset triggered by the Atlantic Niño. *Clim. Dyn.* **44**, 115–131 (2015).
14. Y.-G. Ham, J.-S. Kug, J.-Y. Park, Two distinct roles of Atlantic SSTs in ENSO variability: North Tropical Atlantic SST and Atlantic Niño. *Geophys. Res. Lett.* **40**, 4012–4017 (2013).
15. C. Wang, S.-K. Lee, C. R. Mechoso, Interhemispheric influence of the atlantic warm pool on the southeastern pacific. *J. Climate* **23**, 404–418 (2010).
16. W. Cai, L. Wu, M. Lengaigne, T. Li, S. McGregor, J.-S. Kug, J.-Y. Yu, M. F. Stuecker, A. Santoso, X. Li, Y.-G. Ham, Y. Chikamoto, B. Ng, M. J. McPhaden, Y. Du, D. Dommenget, F. Jia, J. B. Kajtar, N. Keenlyside, X. Lin, J.-J. Luo, M. Martín-Rey, Y. Ruprich-Robert, G. Wang, S.-P. Xie, Y. Yang, S. M. Kang, J.-Y. Choi, B. Gan, G.-I. Kim, C.-E. Kim, S. Kim, J.-H. Kim, P. Chang, Pantropical climate interactions. *Science* **363**, eaav4236 (2019).
17. I. Richter, H. Tokinaga, Y. Kosaka, T. Doi, T. Kataoka, Revisiting the tropical atlantic influence on El Niño–Southern oscillation. *J. Climate* **34**, 8533–8548 (2021).
18. F. Jiang, W. Zhang, F. Jin, M. F. Stuecker, A. Timmermann, M. J. McPhaden, J. Boucharel, A. T. Wittenberg, Resolving the tropical Pacific/Atlantic interaction conundrum. *Geophys. Res. Lett.* **50**, e2023GL103777 (2023).
19. P. Chang, Y. Fang, R. Saravanan, L. Ji, H. Seidel, The cause of the fragile relationship between the Pacific El Niño and the Atlantic Niño. *Nature* **443**, 324–328 (2006).
20. H. Tokinaga, I. Richter, Y. Kosaka, ENSO influence on the Atlantic Niño, revisited: Multi-year versus single-Year ENSO events. *J. Climate* **32**, 4585–4600 (2019).
21. J. F. Lübbecke, M. J. McPhaden, On the inconsistent relationship between pacific and Atlantic Niños*. *J. Climate* **25**, 4294–4303 (2012).
22. F. Kucharski, A. Bracco, J. H. Yoo, F. Molteni, Atlantic forced component of the Indian monsoon interannual variability. *Geophys. Res. Lett.* **35**, L04706 (2008).
23. F. Kucharski, A. Bracco, J. H. Yoo, A. M. Tompkins, L. Feudale, P. Ruti, A. Dell'Aquila, A Gill-Matsuno-type mechanism explains the tropical Atlantic influence on African and Indian monsoon rainfall. *Q. J. Roy. Meteorol. Soc.* **135**, 569–579 (2009).
24. V. Pottapinjara, M. S. Girishkumar, S. Sivareddy, M. Ravichandran, R. Murtugudde, Relation between the upper ocean heat content in the equatorial Atlantic during boreal spring and the Indian monsoon rainfall during June-September. *Int. J. Climatol.* **36**, 2469–2480 (2016).
25. R. K. Yadav, G. Srinivas, J. S. Chowdary, Atlantic Niño modulation of the Indian summer monsoon through Asian jet. *Npj Clim. Atmospheric Sci.* **1**, 23 (2018).
26. L. Zhang, W. Han, Indian ocean dipole leads to atlantic Niño. *Nat. Commun.* **12**, 5952 (2021).
27. H. Liao, C. Wang, Sea surface temperature anomalies in the Western Indian Ocean as a trigger for atlantic Niño Events. *Geophys. Res. Lett.* **48**, e2021GL092489 (2021).
28. H. Tokinaga, S.-P. Xie, Weakening of the equatorial Atlantic cold tongue over the past six decades. *Nat. Geosci.* **4**, 222–226 (2011).
29. A. Prigent, J. F. Lübbecke, T. Bayr, M. Latif, C. Wengel, Weakened SST variability in the tropical Atlantic Ocean since 2000. *Clim. Dyn.* **54**, 2731–2744 (2020).
30. J. F. Lübbecke, B. Rodríguez-Fonseca, I. Richter, M. Martín-Rey, T. Losada, I. Polo, N. S. Keenlyside, Equatorial Atlantic variability—Modes, mechanisms, and global teleconnections. *WIREs Clim. Change.* **9**, e527 (2018).
31. T. Losada, B. Rodríguez-Fonseca, Tropical atmospheric response to decadal changes in the atlantic equatorial mode. *Clim. Dyn.* **47**, 1211–1224 (2016).
32. C. T. Sabeerali, R. S. Ajayamohan, H. K. Bangalath, N. Chen, Atlantic zonal mode: An emerging source of Indian summer monsoon variability in a warming world. *Geophys. Res. Lett.* **46**, 4460–4467 (2019).
33. J. C. H. Chiang, D. J. Vimont, Analogous Pacific and atlantic meridional modes of tropical atmosphere–ocean variability. *J. Climate* **17**, 4143–4158 (2004).
34. I. Richter, S. K. Behera, Y. Masumoto, B. Taguchi, H. Sasaki, T. Yamagata, Multiple causes of interannual sea surface temperature variability in the equatorial Atlantic Ocean. *Nat. Geosci.* **6**, 43–47 (2013).
35. G. R. Foltz, M. J. McPhaden, Interaction between the Atlantic meridional and Niño modes. *Geophys. Res. Lett.* **37**, L18604 (2010).
36. M. Martín-Rey, I. Polo, B. Rodríguez-Fonseca, T. Losada, A. Lazar, Is there evidence of changes in tropical atlantic variability modes under AMO phases in the observational record? *J. Climate* **31**, 515–536 (2018).
37. M. Martín-Rey, B. Rodríguez-Fonseca, I. Polo, F. Kucharski, On the Atlantic–Pacific Niños connection: A multidecadal modulated mode. *Clim. Dyn.* **43**, 3163–3178 (2014).

38. H. C. Nnamchi, M. Latif, N. S. Keenlyside, J. Kjellsson, I. Richter, Diabatic heating governs the seasonality of the Atlantic Niño. *Nat. Commun.* **12**, 376 (2021).
39. S. Gadgil, P. V. Joseph, N. V. Joshi, Ocean-atmosphere coupling over monsoon regions. *Nature* **312**, 141–143 (1984).
40. N. E. Graham, T. P. Barnett, Sea surface temperature, surface wind divergence, and convection over tropical oceans. *Science* **238**, 657–659 (1987).
41. D. E. Waliser, K. M. Lau, J.-H. Kim, The influence of coupled sea surface temperatures on the madden–Julian oscillation: A model perturbation experiment. *J. Atmos. Sci.* **56**, 333–358 (1999).
42. W. Zhang, F. Jiang, M. F. Stuecker, F.-F. Jin, A. Timmermann, Spurious North Tropical Atlantic precursors to El Niño. *Nat. Commun.* **12**, 3096 (2021).
43. J. Bjerknes, Atmospheric teleconnections from the equatorial Pacific. *Mon. Weather Rev.* **97**, 163–172 (1969).
44. V. Eyring, S. Bony, G. A. Meehl, C. A. Senior, B. Stevens, R. J. Stouffer, K. E. Taylor, Overview of the coupled model intercomparison project phase 6 (CMIP6) experimental design and organization. *Geosci. Model Dev.* **9**, 1937–1958 (2016).
45. C. Wang, L. Zhang, S.-K. Lee, L. Wu, C. R. Mechoso, A global perspective on CMIP5 climate model biases. *Nat. Clim. Change* **4**, 201–205 (2014).
46. L. Svendsen, N. G. Kvamstø, N. Keenlyside, Weakening AMOC connects Equatorial Atlantic and Pacific interannual variability. *Clim. Dyn.* **43**, 2931–2941 (2014).
47. I. Polo, B. W. Dong, R. T. Sutton, Changes in tropical Atlantic interannual variability from a substantial weakening of the meridional overturning circulation. *Clim. Dyn.* **41**, 2765–2784 (2013).
48. Y. Yang, L. Wu, W. Cai, F. Jia, B. Ng, G. Wang, T. Geng, Suppressed Atlantic Niño/Niña variability under greenhouse warming. *Nat. Clim. Change* **12**, 814–821 (2022).
49. L. R. Crespo, A. Prigent, N. Keenlyside, S. Koseki, L. Svendsen, I. Richter, E. Sánchez-Gómez, Weakening of the Atlantic Niño variability under global warming. *Nat. Clim. Change* **12**, 822–827 (2022).
50. P. Silva, I. Wainer, M. Khodri, Changes in the equatorial mode of the tropical atlantic in terms of the Bjerknes feedback index. *Clim. Dyn.* **56**, 3005–3024 (2021).
51. Y. Okumura, S.-P. Xie, Some overlooked features of tropical atlantic climate leading to a new niño-like phenomenon. *J. Climate* **19**, 5859–5874 (2006).
52. I. Richter, S. K. Behera, Y. Masumoto, B. Taguchi, N. Komori, T. Yamagata, On the triggering of Benguela Niños: Remote equatorial versus local influences. *Geophys. Res. Lett.* **37**, L20604 (2010).
53. J. F. Lübbecke, C. W. Böning, N. S. Keenlyside, S.-P. Xie, On the connection between Benguela and equatorial Atlantic Niños and the role of the South Atlantic Anticyclone. *J. Geophys. Res.* **115**, C09015 (2010).
54. N. A. Rayner, D. E. Parker, E. B. Horton, C. K. Folland, L. V. Alexander, D. P. Rowell, E. C. Kent, A. Kaplan, Global analyses of sea surface temperature, sea ice, and night marine air temperature since the late nineteenth century. *J. Geophys. Res.* **108**, 4407 (2003).
55. H. Hersbach, W. Bell, P. Berrisford, A. Horányi, J. M. Sabater, J. Nicolas, R. Radu, D. Schepers, A. Simmons, C. Soci, D. Dee, in *Global reanalysis: Goodbye ERA-Interim, Hello ERA5* (ECMWF, 2019), pp. 17–24.
56. H. Zuo, M. Alonso-Balmaseda, K. Mogensen, S. Tietsche, *OCEAN5: The ECMWF Ocean Reanalysis System and Its Real-Time Analysis Component* (ECMWF, 2018).
57. L. Cheng, J. Abraham, G. Goni, T. Boyer, S. Wijffels, R. Cowley, V. Gouretski, F. Reseghetti, S. Kizu, S. Dong, F. Bringas, M. Goes, L. Houpert, J. Sprintall, J. Zhu, XBT Science: Assessment of instrumental biases and errors. *Bull. Am. Meteorol. Soc.* **97**, 924–933 (2016).
58. C. Deser, A. S. Phillips, M. A. Alexander, Twentieth century tropical sea surface temperature trends revisited. *Geophys. Res. Lett.* **37**, L10701 (2010).
59. K. Takahashi, A. Montecinos, K. Goubanova, B. Dewitte, ENSO regimes: Reinterpreting the canonical and Modoki El Niño. *Geophys. Res. Lett.* **38**, L10704 (2011).
60. D. J. Vimont, M. A. Alexander, M. Newman, Optimal growth of central and east pacific ENSO events. *Geophys. Res. Lett.* **41**, 4027–4034 (2014).
61. L. Zhang, W. Han, Barrier for the Eastward Propagation of Madden-Julian oscillation over the maritime continent: A possible new mechanism. *Geophys. Res. Lett.* **47**, e2020GL090211 (2020).
62. E. Roeckner, K. Arpe, L. Bengtsson, M. Christoph, M. Claussen, L. Dumenil, M. Esch, M. Giorgetta, U. Schlese, U. Schulzweida, L. Dümenil, in *The Atmospheric General Circulation Model ECHAM-4: Model Description and Simulation of Present-Day Climate* (Max-Planck-Institut für Meteorologie, 1996).
63. K. Riahi, D. P. van Vuuren, E. Kriegler, J. Edmonds, B. C. O'Neill, S. Fujimori, N. Bauer, K. Calvin, R. Dellink, O. Fricko, W. Lutz, A. Popp, J. C. Cuaresma, S. Kc, M. Leimbach, L. Jiang, T. Kram, S. Rao, J. Emmerling, K. Ebi, T. Hasegawa, P. Havlik, F. Humpenöder, L. A. Da Silva, S. Smith, E. Stehfest, V. Bosetti, J. Eom, D. Gernaat, T. Masui, J. Rogelj, J. Strefler, L. Drouet, V. Krey, G. Luderer, M. Harmsen, K. Takahashi, L. Baumstark, J. C. Doelman, M. Kainuma, Z. Klimont, G. Marangoni, H. Lotze-Campen, M. Obersteiner, A. Tabeau, M. Tavoni, The shared socioeconomic pathways and their energy, land use, and greenhouse gas emissions implications: An overview. *Glob. Environ. Change* **42**, 153–168 (2017).
64. P. R. Gent, G. Danabasoglu, L. J. Donner, M. M. Holland, E. C. Hunke, S. R. Jayne, D. M. Lawrence, R. B. Neale, P. J. Rasch, M. Vertenstein, P. H. Worley, Z. L. Yang, M. Zhang, The community climate system model version 4. *J. Climate* **24**, 4973–4991 (2011).

Acknowledgments: We acknowledge the modeling groups, the Program for Climate Model Diagnosis and Intercomparison (PCMDI), and the World Climate Research Programme (WCRP) for their roles in making available CMIP6 datasets. Part of the work was completed while W.H. was visiting the International Space Science Institute (ISSI), Bern, Switzerland. W.H. thanks the Johannes Geiss Fellowship from ISSI for providing travel support. **Funding:** This work was supported by the National Natural Science Foundation of China (42192564), the National Key R&D Program of China (2019YFA0606701), the Strategic Priority Research Program of the Chinese Academy of Sciences (XDB42000000), and the Development Fund of South China Sea Institute of Oceanology of the Chinese Academy of Sciences (SCSIO202208) (to C.W.); the South China Sea Institute of Oceanology (grant LTORC2201) and Development fund of South China Sea Institute of Oceanology of the Chinese Academy of Sciences (SCSIO202203) (to L.Z.); the NOAA Office of Oceanic and Atmospheric Research Climate Program Office (CPO), NA20OAR4310480 (to W.H.); the Regional and Global Model Analysis (RGMA) component of the Earth and Environmental System Modeling Program of the U.S. Department of Energy's Office of Biological and Environmental Research (BER) via the National Science Foundation (NSF) IA 1947282 (DE-SC0022070); PMEL, contribution no. 5430 (to M.J.M.); and South China Sea Institute of Oceanology, grant LTORC2202 (to W.X.). The National Center for Atmospheric Research is sponsored by the NSF of the United States of America under cooperative agreement no. 1852977 (to A.H.). **Author contributions:** L.Z. conceived the study and wrote the initial manuscript in discussion with C.W. L.Z. conducted the analysis and prepared the figures. All the authors contributed to interpretating results and improving the paper. **Competing interests:** The authors declare that they have no competing interests. **Data and materials availability:** All data needed to evaluate the conclusions in the paper are present in the paper and/or the Supplementary Materials. The observational data and climate model simulations used in this study are publicly available and can be downloaded from the following websites: HadISST (www.metoffice.gov.uk/hadobs/hadisst/), ERA5 (www.ecmwf.int/en/forecasts/dataset/ecmwf-reanalysis-v5), ORAS5 (https://cds.climate.copernicus.eu/cdsapp#!/dataset/reanalysis-oras5?tab=form), CMIP6 (https://esgf-node.llnl.gov/projects/cmip6/), and CCSM4 (www.cesm.ucar.edu/experiments/cesm1.0/). The AGCM results are available at https://scholar.colorado.edu/concern/datasets/ks65hd74b.

Submitted 4 May 2023
Accepted 21 September 2023
Published 25 October 2023
10.1126/sciadv.adi5507

ScienceAdvances

Emergence of the Central Atlantic Niño

Lei Zhang, Chunzai Wang, Weiqing Han, Michael J. McPhaden, Aixue Hu, and Wen Xing

Sci. Adv. **9** (43), eadi5507. DOI: 10.1126/sciadv.adi5507